University of Groningen

Enormous disc of cool gas surrounding the nearby powerful radio galaxy NGC 612 (PKS 0131-36)

Emonts, B. H. C.; Morganti, R.; Oosterloo, T. A.; Holt, J.; Tadhunter, C. N.; van der Hulst, J. M.; Ojha, R.; Sadler, E. M.

Published in:
Monthly Notices of the Royal Astronomical Society

DOI:
10.1111/j.1365-2966.2008.13142.x

IMPORTANT NOTE: You are advised to consult the publisher's version (publisher's PDF) if you wish to cite from it. Please check the document version below.

Document Version
Publisher's PDF, also known as Version of record

Publication date:
2008

Link to publication in University of Groningen/UMCG research database

Citation for published version (APA):
Emonts, B. H. C., Morganti, R., Oosterloo, T. A., Holt, J., Tadhunter, C. N., van der Hulst, J. M., ... Sadler, E. M. (2008). Enormous disc of cool gas surrounding the nearby powerful radio galaxy NGC 612 (PKS 0131-36). Monthly Notices of the Royal Astronomical Society, 387(1), 197-208. https://doi.org/10.1111/j.1365-2966.2008.13142.x

Copyright
Other than for strictly personal use, it is not permitted to download or to forward/distribute the text or part of it without the consent of the author(s) and/or copyright holder(s), unless the work is under an open content license (like Creative Commons).

Take-down policy
If you believe that this document breaches copyright please contact us providing details, and we will remove access to the work immediately and investigate your claim.

Downloaded from the University of Groningen/UMCG research database (Pure): http://www.rug.nl/research/portal. For technical reasons the number of authors shown on this cover page is limited to 10 maximum.

Download date: 22-05-2019

Mon. Not. R. Astron. Soc. **387,** 128–136 (2008) doi:10.1111/j.1365-2966.2008.13019.x

Alignment of voids in the cosmic web

Erwin Platen,* Rien van de Weygaert and Bernard J. T. Jones
Kapteyn Astronomical Institute, University of Groningen, PO Box 800, 9700 AV Groningen, the Netherlands

Accepted 2008 January 16. Received 2007 December 20; in original form 2007 November 15

ABSTRACT

We investigate the shapes and mutual alignment of voids in the large-scale matter distribution of a Λ cold dark matter (ΛCDM) cosmology simulation. The voids are identified using the novel watershed void finder (WVF) technique. The identified voids are quite non-spherical and slightly prolate, with axis ratios in the order of $c : b : a \approx 0.5 : 0.7 : 1$. Their orientations are strongly correlated with significant alignments spanning scales $>30\,h^{-1}$ Mpc.

We also find an intimate link between the cosmic tidal field and the void orientations. Over a very wide range of scales we find a coherent and strong alignment of the voids with the tidal field computed from the smoothed density distribution. This orientation–tide alignment remains significant on scales exceeding twice the typical void size, which shows that the long-range external field is responsible for the alignment of the voids. This confirms the view that the large-scale tidal force field is the main agent for the large-scale spatial organization of the cosmic web.

Key words: methods: data analysis – methods: numerical – cosmology: theory – large-scale structure of Universe.

1 INTRODUCTION

Galaxy redshift surveys and computer simulations of cosmic structure formation have shown that matter traces out a frothy pattern, the cosmic web. Bond, Kofman & Pogosyan (1996) established how the tidal forces induced by the inhomogeneous cosmic matter distribution are the main agent shaping the Cosmic Web. The resulting cosmic tidal force field is the source of the large-scale, coherent, anisotropic forces which shape the cosmic matter distribution into characteristic filamentary and sheet-like patterns.

Voids are a dominant component of the cosmic web (see e.g. Romano-Díaz & van de Weygaert 2007; Tully et al. 2007), occupying most of the volume of space. In this paper we present evidence for significant alignments between neighbouring voids and establish the intimate dynamic link between voids and the cosmic tidal force field. The watershed void finder (WVF) procedure (Platen, van de Weygaert & Jones 2007) that we use to identify voids is crucial to the success of this analysis. The WVF technique is based on the topological characteristics of the spatial density field and thereby provides objectively defined measures for the size, shape and orientation of void patches.

Large voids form around deep density troughs in the primordial density field. The main aspects of the evolution of a large void may be understood on the basis of the expansion of simple spherical and isolated underdensities (e.g. Bertschinger 1985). Underdense regions expand with respect to the background Universe and in general will have the tendency to grow more spherical with time (Icke 1984). However, Shandarin et al. (2006) and Park & Lee (2007a) have emphasized that, in realistic cosmological circumstances, voids will be non-spherical. This is quite apparent in images of, for example, the Millennium Simulation (Springel et al. 2005). Moreover, substructures within voids display a manifest alignment along a preferred direction. This is, in part, a consequence of the relatively strong influence of the surrounding inhomogeneous matter distribution on the void's structure and evolution.

Voids evolve hierarchically: as they expand with respect to the background Universe they merge with their surrounding peers, building voids of ever larger sizes (Regøs & Geller 1991; van de Weygaert & van Kampen 1993; Gottlöber et al. 2003; Colberg et al. 2005). Small voids can survive as substructure within the larger voids or may disappear under the gravitational impact of surrounding overdense structures (Sahni, Sathyaprakash & Shandarin 1994; Sheth & van de Weygaert 2004). The result is a void population whose scale is distributed around a characteristic void size: we shall show this using our WVF sample.

A major manifestation of large-scale tidal influences is that of the alignment of shape and angular momentum of objects (see Bond et al. 1996; Desjacques 2007). The alignment of the orientations of galaxy haloes, galaxy spins and clusters with larger scale structures such as clusters, filaments and superclusters has been the subject of numerous studies (see e.g. Binggeli 1982; Bond 1987; Rhee, van Haarlem & Katgert 1991; Plionis & Basilakos 2002; Basilakos et al. 2006; Trujillo, Carretero & Patiri 2006; Aragón-Calvo et al. 2007; Lee & Evrard 2007; Lee et al. 2007; Park & Lee 2007b). Recent analytical and numerical work by Park & Lee (2007a) discussed the magnitude of the tidal contribution to the shape of voids (see also Lee & Park 2006). Describing the evolution of voids under the influence

*E-mail: platen@astro.rug.nl

© 2008 The Authors. Journal compilation © 2008 RAS

Downloaded from https://academic.oup.com/mnras/article-abstract/387/1/128/998214 by University Library user on 19 December 2018

of tidal fields by means of the Lagrangian Zel'dovich approximation, they found that the ellipticity distribution of voids is a sensitive function of various cosmological parameters and remarked that the shape evolution of voids provides a remarkably robust constraint on the dark energy equation of state (Lee & Park 2007).

In Section 2 we introduce the *N*-body simulation which we used to identify the voids, along with a brief description of the WVF method we use to identify the voids in our sample. The results for individual void characteristics, in particular the size and shape of voids, are presented in Section 3. Then in Section 4 we present the analysis of the alignment of voids in the sample. The possible origins for the void alignment are discussed in Section 5, and in Section 6 we focus on the role of tidal fields in determining the evolutionary history of voids. Finally, Section 7 concludes with a short discussion and prospects.

2 THE VOID SAMPLE

It is essential to have a statistically representative void sample for our study of the shapes of voids and their relative alignment. We also need a sufficiently large spatial coverage in order to evaluate tidal field contributions over a large range of scales. Thus it is necessary to have a simulation with a large box size. We used the Very Large Simulation (VLS) from the Virgo Supercomputing Consortium,[1] a simulation of cosmic structure formation in a ΛCDM cosmology with $\Omega_{\rm m,0} = 0.3$, $\Omega_{\Lambda,0} = 0.7$, $H_0 = 70\,{\rm km\,s^{-1}\,Mpc^{-1}}$ and $\sigma_8 = 0.9$. The simulation contains 512^3 *N*-body particles, each with a mass of $6.86 \times 10^{10}\,h^{-1}\,{\rm M}_\odot$ in a comparatively large box of side $479\,h^{-1}$ Mpc. We used the particle distribution at the final time-step, corresponding to the current cosmic epoch $a = 1$.

2.1 Void identification

The particle distribution of the simulation is converted into a grid-based density field by means of Delaunay Tessellation Field Estimator (DTFE; van de Weygaert & Schaap 2007). The key feature of DTFE is that it is a reconstruction method that does not involve any user-defined parameters. Moreover, its natural and intrinsic filtering and interpolation procedure yields a density field that remains faithful to both the density and shape structure of the original particle distribution. DTFE guarantees an optimal representation of the geometry and topology of the web-like patterns in the mass distribution. A slice through the DTFE resampled density field is shown in the first panel of Fig. 1.

After resampling the point density distribution with DTFE, we applied the WVF (Platen, van de Weygaert & Jones 2007) in order to identify the voids in the simulation. The WVF procedure traces the basin and its encompassing boundary for each minimum in the spatial mass distribution. Because WVF is free of any a priori shape criterion it is ideally suited to analysing the morphology of underdense regions in the cosmic web.

The WVF procedure works as follows (see Platen, van de Weygaert & Jones 2007, for a detailed description). First, we remove shot noise effects in the raw DTFE density field by smoothing at the Nyquist scale ($\approx 1.0\,h^{-1}$ Mpc); this is done using a Butterworth $n = 2$ filter. Then we identify the minima in the resulting density field and tag each minimum with a unique identification number. We can visualize the density field as a landscape with basins around each minimum. Starting from the minima we flood this landscape. As the flood level rises the basins surrounding each minimum start to fill up. Walls gradually emerge along the crest lines of the density field at the interstices between distinct regions. The final product of the procedure will be a division of the density field into individual void cells.

[1] The Virgo Consortium VLS Λ cold dark matter (ΛCDM) data are available at http://www.mpa-garching.mpg.de/galform/virgo/vls/

3 VOID CHARACTERISTICS

In the first panel of Fig. 1 each void identified by WVF is indicated by the solid black line marking the surrounding void boundary. The image shows that we indeed have a large number of voids in our sample. In the upper right-hand panel we zoom in on a region of the simulation box (the white box in first panel) which we use for the purpose of illustrating the subsequent steps (the analysis is done on the entire box). The upper right-hand panel also has lines indicating the (projected) magnitude and direction of the major axis of each void. Visual inspection of the void regions in this panel manifestly suggests some degree of alignment. Quantitative analysis will establish the significance of that alignment.

3.1 Void size

The size and shape distribution of the WVF-identified voids is shown in Fig. 2. In the simulation we found 29 000 voids, with an average void size $R_{\rm v} \approx 8.5\,h^{-1}$ Mpc. We defined the void size R as the radius of a sphere which has the same volume as the void region. This volume is calculated by a direct integration of all the grid volume elements contained inside the void. The void size distribution in Fig. 2, first panel, clearly shows a peak in the size distribution, confirming the prediction by Sheth & van de Weygaert (2004).

3.2 Void shape

For each individual void region we calculate the shape tensor $\boldsymbol{S}_{ij}$ by summing over the N volume elements k located within the void:

$$\boldsymbol{S}_{ij} = -\sum_k x_{ki} x_{kj} \qquad \text{(off-diagonal)},$$
$$\boldsymbol{S}_{ii} = \sum_k \left(\boldsymbol{x}_k^2 - x_{ki}^2\right) \qquad \text{(diagonal)}, \tag{1}$$

where $\boldsymbol{x}_k$ is the position of the kth volume element within the void, with respect to the (volume-weighted) void centre $\bar{\boldsymbol{r}}_{\rm v}$, i.e. $\boldsymbol{x}_k = \boldsymbol{r}_k - \bar{\boldsymbol{r}}_{\rm v}$. The shape tensor $\boldsymbol{S}_{ij}$ is related to the inertia tensor $\boldsymbol{I}_{ij}$. However, it differs in assigning equal weight to each volume element within the void region. Instead of biasing the measure towards the mass concentrations near the edge of voids, the shape tensor $\boldsymbol{S}_{ij}$ yields a truer reflection of the void's interior shape.

When evaluating alignments we will mostly use the traceless version of the shape tensor:

$$\tilde{\boldsymbol{S}}_{ij} = \boldsymbol{S}_{ij} - \frac{1}{3}\boldsymbol{S}\,\delta_{ij}, \qquad \boldsymbol{S} = \sum_k \boldsymbol{S}_{kk}. \tag{2}$$

The length and orientation of the shape ellipsoid are inferred from the eigenvalues and eigenvectors of $\boldsymbol{S}_{ij}$. The eigenvalues of the void ellipsoid are labelled so that $s_1 > s_2 > s_3$. The corresponding semi-axes are oriented along the directions of the corresponding unit eigenvectors $\hat{\boldsymbol{e}}_{s_1}$, $\hat{\boldsymbol{e}}_{s_2}$ and $\hat{\boldsymbol{e}}_{s_3}$. The length of the semi-axes a_i are

$$a_1^2 = \frac{5}{2N}\,(s_2 + s_3 - s_1) \tag{3}$$

with cyclic permutation for the other axes (N is the number of volume elements within the void). The longest axis is directed along $\hat{\boldsymbol{e}}_{s_1}$, the shortest along $\hat{\boldsymbol{e}}_{s_3}$.

Downloaded from https://academic.oup.com/mnras/article-abstract/387/1/128/998214 by University Library user on 19 December 2018

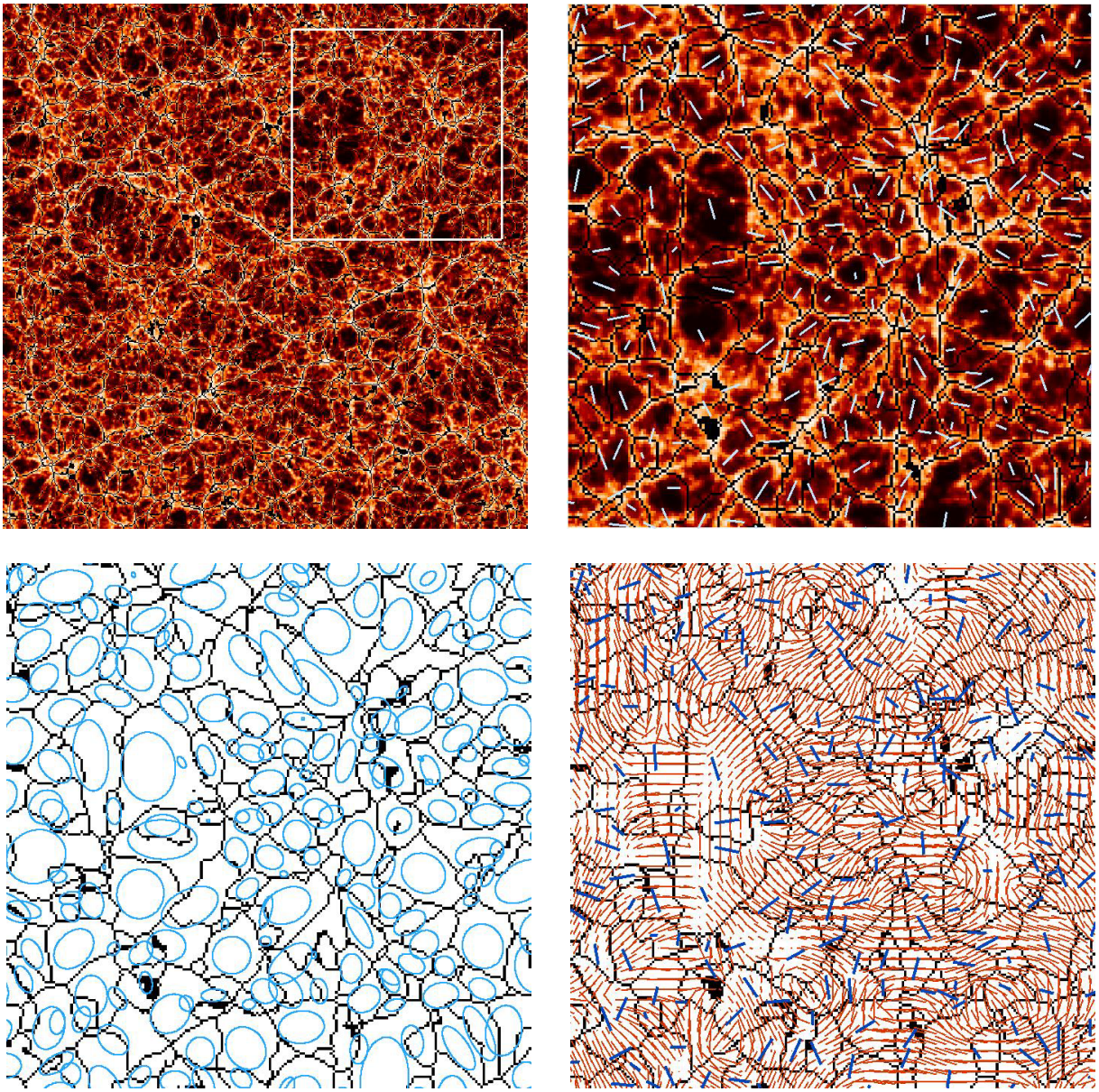

Figure 1. The four panels show a slice through the density field with the void segmentation superposed. The first panel shows a slice through the density field of the whole simulation box. The density field is determined by DTFE. Superimposed are the black solid lines indicating the boundaries of the WVF voids. The white box indicates the section which forms the subject of the next three frames. Second panel: density field in the subbox with the WVF void boundaries superimposed (solid lines). The blue bars indicate the direction of the projection of the longest void axis. Third panel: the WVF void boundary contours (solid lines) with the fitted void shape ellipsoids superimposed. Fourth panel: on the landscape with WVF void boundaries the tidal field compressional component is represented by tidal bars (red), representing the direction and strength of the tidal field. Also depicted are the void shape bars (blue).

We quantify the shape of the void ellipsoids in terms of the two axis ratios $\eta_{21} = a_2/a_1$ and $\eta_{32} = a_3/a_2$. Amongst the triaxial void ellipsoids we make a distinction between oblate ones, with $\eta_{21} > \eta_{32}$, and prolate ones having $\eta_{21} < \eta_{32}$. If voids were spherical we would have $\eta_{21} = \eta_{32} = 1$ (though, in reality, perfect sphericity does not exist).

3.3 Results on void shapes

In the density field in the upper right-hand frame of Fig. 1 we have indicated the projected direction of the longest axis of the voids by means of a bar along the corresponding eigenvector, with the length of the bar proportional to the size of the void axis. It allows a superficial comparison with the related WVF void patches (indicated by the solid black lines marking their boundary).

The lower left-hand panel of Fig. 1 shows the shape ellipsoids of each void within the region of the simulation box shown in the top right-hand panel. The centres of the shape ellipsoids are located at the centre of each void with their size scaled according to match the void volume: they give a convenient visual impression of the void shapes and sizes. The reasonably accurate degree to which the ellipsoids reflect the shape of the voids may be inferred from a comparison with the WVF void regions themselves.

Downloaded from https://academic.oup.com/mnras/article-abstract/387/1/128/998214 by University Library user on 19 December 2018

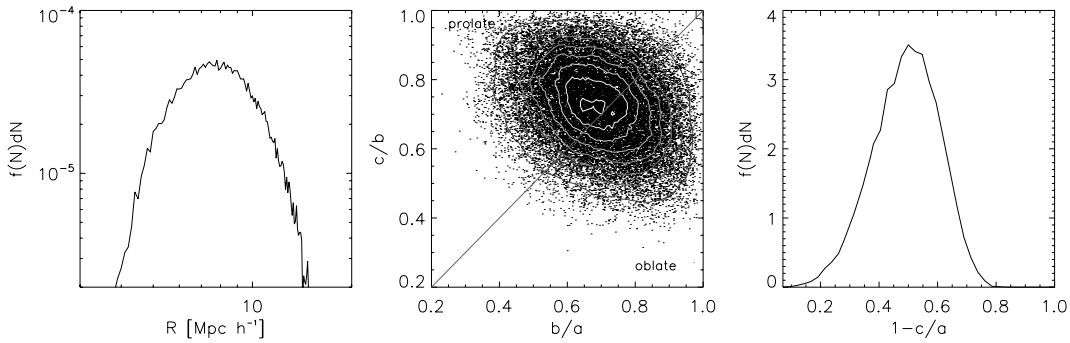

Figure 2. Void characteristics and statistics. Left: the (peaked) void size distribution as a function of void radius $R_{\rm v}$. Centre: scatter diagram of the two void axis ratios $\eta_{32} = a_3/a_2$ versus $\eta_{21} = a_2/a_1$. Right: distribution of void ellipticity $\epsilon = 1 - a_3/a_1$.

Clearly, the voids are quite non-spherical. A more quantitative impression of the shape distribution may be found in the second and third panel of Fig. 2 which show that the voids are far from spherical.

The intrinsic triaxial shape of voids is apparent from the distribution in the second panel of Fig. 2. This shows a scatter plot of the two axis ratios, η_{12} versus η_{23} for every void in the sample. To guide the eye we have superimposed the inferred isodensity contours defined by the point density in the scatter plot. We find a slight asymmetry: there are more prolate voids than oblate ones.

The third panel shows that the distribution of the ellipticity $\epsilon = 1 - a_3/a_1$ is skewed towards higher values of $\epsilon > 0.5$. The void population is marked by pronounced triaxial shapes: the average ratio between the smallest and largest axis $c/a \approx 0.49$. This ratio agrees well with the value of 0.45 found by Shandarin et al. (2006) (which is perhaps a little surprising given the totally different void definitions used in that paper).

In summary, we find voids to be slightly prolate, with average axis ratios in the order of $c : b : a \approx 0.5 : 0.7 : 1$.

Two important factors contribute to this flattening. Even though, internally, voids tend to become more spherical as they expand (Icke 1984), perfect sphericity will hardly ever be reached. Before voids would be able to become spherical they would encounter surrounding structures such as overdense filaments or planar walls. Even more important may be the fact that, for voids, external tidal influences are particularly important: voids will always be rather moderate underdensities since they can never be more underdense than $\delta = -1$. The external tidal forces drive a significant anisotropy in the development of the voids, and in the extreme cases may cause complete collapse of the void along one or more of its axes. This is another aspect of the way in which tidal forces shape the cosmic web, as has been emphasized by Bond et al. (1996).

4 VOID ALIGNMENTS

Large-scale influences play a major role not only in shaping individual voids but also on their mutual arrangement and organization. A particularly important manifestation of this is the mutual alignment between voids. In this section we establish the significance of this effect, and in the next section we analyse the correlation between the tidal force field and the void orientation.

4.1 Void alignments: definitions

We take the void centres in our sample to define a spatial point process. Three void alignment measures have been investigated. Each is a marked correlation function (Stoyan & Stoyan 1994; Beisbart & Kersher 2000) and assesses the degree of alignment as a function of the distance r between the void centres. The mark for each void pair is the cosine of the angles between two specific axes of the void or a combination of these.

The first alignment measure is the full shape correlation $\boldsymbol{A}_{\rm SS}$. The second measure concerns the alignment strength $\boldsymbol{A}_{33}$ between the longest axes of the voids, and the third measure concerns the alignment strength A_{11} between the shortest axes of the voids. To determine these functions we evaluate the alignment between each pair of voids as a function of the separation of their centres r.

The alignment between a pair of voids m and n, with traceless shape tensors $\tilde{\boldsymbol{S}}_{m,ij}$ and $\tilde{\boldsymbol{S}}_{n,ij}$, is specified in terms of the following set of quantities:

$$\begin{aligned}
\Gamma_{\rm SS}(m,n) &= \frac{\sum_{i,j} \tilde{\boldsymbol{S}}_{m,ij}\, \tilde{\boldsymbol{S}}_{n,ij}}{\tilde{\boldsymbol{S}}_m\, \tilde{\boldsymbol{S}}_n}, \\
\Gamma_{11}(m,n) &= \hat{\boldsymbol{e}}_{s_1}(m) \cdot \hat{\boldsymbol{e}}_{s_1}(n), \\
\Gamma_{22}(m,n) &= \hat{\boldsymbol{e}}_{s_2}(m) \cdot \hat{\boldsymbol{e}}_{s_2}(n), \\
\Gamma_{33}(m,n) &= \hat{\boldsymbol{e}}_{s_3}(m) \cdot \hat{\boldsymbol{e}}_{s_3}(n),
\end{aligned} \tag{4}$$

in which $\tilde{\boldsymbol{S}}_m$ and $\tilde{\boldsymbol{S}}_n$ are the norms of the corresponding (traceless) shape ellipsoids. In essence Γ_{11}, Γ_{22} and Γ_{33} are the cosines of the angles between the corresponding void axes, directed along the shape eigenvectors $\hat{\boldsymbol{e}}_{s_1}, \hat{\boldsymbol{e}}_{s_2}$ and $\hat{\boldsymbol{e}}_{s_3}$. These alignment measures do not depend on the degree of ellipticity of each void, they focus exclusively on the relative orientation of the void axes.

The corresponding marked correlation functions are an expression of the strength of the alignments as a function of distance r between the void centres:

$$\begin{aligned}
&\boldsymbol{C}_{\rm SS}(r) = \langle\, \Gamma_{\rm SS}\, \rangle, \\
&\boldsymbol{C}_{11}(r) = \langle\, \Gamma_{11}\, \rangle,\ \boldsymbol{C}_{22}(r) = \langle\, \Gamma_{22}\, \rangle,\ \boldsymbol{C}_{33}(r) = \langle\, \Gamma_{33}\, \rangle.
\end{aligned} \tag{5}$$

The brackets indicate the ensemble average over all void pairs (m, n) whose mutual separation r lies within a band $\Delta\, r$ around r, $|\overline{\boldsymbol{r}}_m - \overline{\boldsymbol{r}}_n| \in [r, r + \Delta r]$. In practice, we bin the void pairs in our void sample into bins which each contain 5000 pairs. This ensures that each bin has equal statistical significance.

Note that because the angle between the corresponding void ellipsoid axes of two voids m and n has a value in the range $0 \leqslant \theta(m,n) \leqslant \pi/2$, the alignment $\Gamma_{ii}(m, n)$ between these two voids lies within the range $0 \leqslant \Gamma_{ii}(m,n) = \cos\theta_{mn} \leqslant 1$. Each of the axis correlation functions $\boldsymbol{C}_{ii} (i = 1, 2, 3)$ is the average cosine between corresponding two void axes, $\boldsymbol{C}_{ii} = \langle \cos\theta \rangle$. For a perfectly randomly oriented sample we would therefore expect $\boldsymbol{C}_{11} = \boldsymbol{C}_{22} = \boldsymbol{C}_{33} = 0.5$. In the case of perfect alignment we would obtain $\boldsymbol{C}_{ii} = 1.0$. A value of

Downloaded from https://academic.oup.com/mnras/article-abstract/387/1/128/998214 by University Library user on 19 December 2018

$C_{ii} \approx 0$ would suggest an anti-alignment, a cross pattern, corresponding to an orientation angle $\theta_{mn} \approx \pi/2$.

4.2 Void alignments: significance

We can gain insight into the significance of the values of the alignment measures $\boldsymbol{C}_{ii}$ by comparing the values obtained for a sample of vectors in which a perfectly aligned subset is mixed with an entirely randomly oriented set of voids.

In this comparison sample, suppose a fraction $f_{\rm r}$ of the void sample has a random orientation while the remaining fraction $f_{\rm a} = 1 - f_{\rm r}$ has a singular orientation along one direction. We may then infer the implied random fraction $f_{\rm r}$ in the comparison sample for the obtained values for $\boldsymbol{C}_{ii}$ in our real void sample.

It is straightforward to infer the implied values of the alignment measures $\boldsymbol{C}_{ii}$ in the comparison sample:

$$\begin{aligned} \boldsymbol{C}_{ii} &= \langle \cos\theta \rangle = 0.5 f_{\rm r}^2 + f_{\rm r} f_{\rm a} + f_{\rm a}^2 \\ &= 0.5\,(f_{\rm r} - 1)^2 + 0.5. \end{aligned} \tag{6}$$

For example, if we were to have 20 per cent aligned voids mixed with 80 per cent random ones, the alignment would be $\boldsymbol{C}_{ii} = 0.52$. An alignment of $\boldsymbol{C}_{ii} = 0.63$ would correspond to ≈50 per cent aligned and ≈50 per cent random voids, while $\boldsymbol{C}_{ii} = 0.75$ would imply ≈70 per cent aligned and ≈30 per cent random ones.

4.3 Void alignments: results

Fig. 3 presents the results for the measured correlations of the void orientations. Each curve corresponds to the orientation correlation between one of the three void axes of voids: the solid black curve to that of the longest axis, $\boldsymbol{C}_{33}$, the dot–dashed curve to that of the shortest axis, $\boldsymbol{C}_{11}$, and the intermediate axis $\boldsymbol{C}_{22}$ (dashed curve).

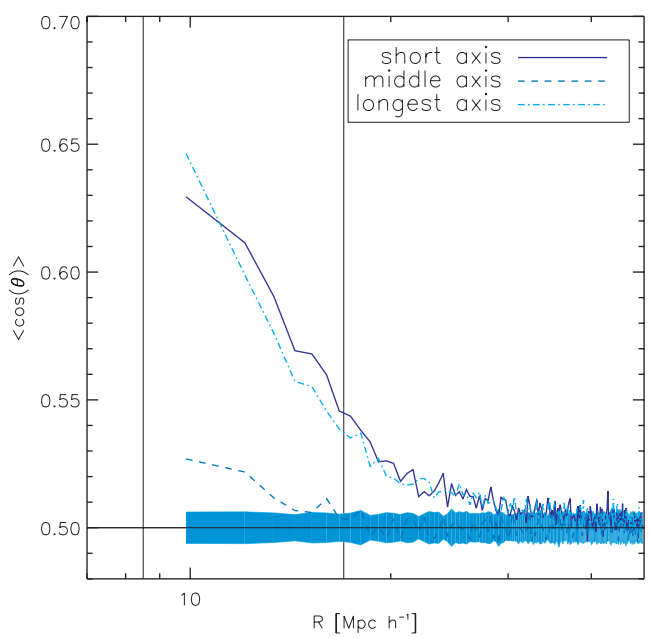

Figure 3. The alignment of the three void axes. The figure shows the (marked) correlation functions $\boldsymbol{C}_{11}(r)$ (solid), $\boldsymbol{C}_{22}(r)$ (dashed) and $\boldsymbol{C}_{33}(r)$ (dot–dashed), the ensemble average of the cosine of the angle between the longest, medium and shortest axes of voids at a distance r. A pure random orientation corresponds to $\boldsymbol{C}_{ii}(r) = 0.50$, a perfectly aligned one $\boldsymbol{C}_{ii}(r) = 1$. The coloured bar around the value $\boldsymbol{C}_{ii} = 0.50$ indicates the 2σ dispersion of a similar random sample.

The figure shows the longest and the smallest axis exhibit the strongest alignment. At short distances their alignment is very strong and remains substantial out to relatively large radii of 20–30 h^{-1} Mpc. Beyond this distance the alignment rapidly declines towards random values. At the smallest distances probed the alignment of the longest and shortest axis reaches values of around 0.65. This corresponds to a random component of only 30 per cent, in combination with 70 per cent perfectly aligned voids. By contrast, the second axis shows a striking lack of alignment on all scales and, except at the shortest separations, appears to be mostly randomly oriented. This is partially due to the considerable scatter in the orientation of the intermediate axis. This may be a reflection of the crudeness of approximating the void shapes by ellipsoids. However, even taking account of the implied scatter the intermediate axis remains more weakly correlated.

To provide an estimate of the significance of the results we have estimated the standard deviation expected for a sample of perfect randomly oriented voids. The 2σ spread is depicted by means of the coloured bar around the expectation value for a random sample, $C_{ii} = 0.5$. We obtained these estimates by a Monte Carlo experiment in which we randomly shuffled the shape ellipsoids over the voids and subsequently remeasured the alignment. Note that the variance remains nearly constant over the whole range. This is a consequence of our decision to define bins having equal number of particles per bin.

5 THE CAUSE OF VOID ALIGNMENT

The possibility that the alignment may be an artefact of the WVF method has to be considered: large spherical voids that were chopped in half would provide an anisotropic void set in which neighbouring voids were strongly aligned. However, this it can quickly be eliminated simply by examining Fig. 1 which shows no such phenomenon. We shall later on present further evidence based on tidal fields that WVF is not itself the source of the alignment.

The reason for the alignment between voids may be due to any of a number of physical effects. Here, we consider three possible physical sources for this alignment: (1) the initial conditions, (2) the geometric packing of the voids and (3) the large-scale tidal field.

5.1 Initial conditions

The first possibility, that the structural correlations are born with the primordial density field, is difficult to address since, at least in the linear regime, the present matter distribution is a direct reflection of those initial conditions. Thus the density fluctuations and the tidal fields that distort them are both present initially, either being deducible from the other. The cosmic web, voids, galaxy haloes as well as the tidal field are all manifestations of the same initial matter distribution.

Voids emerge out of a primordial Gaussian density field. Density peaks and dips in a Gaussian random field are not only clustered (Bardeen et al. 1986), they are also mutually aligned (Bond 1987). This alignment stretches out over scales over which they possess a non-zero correlation function, approximately the same range as that of the comparable population of rich clusters. Even when their evolution would not be influenced by external forces the voids would retain the memory of their initial configuration. Their initial shape would be (slightly) attenuated by their internally driven expansion and the void would keep its initial orientation.

The primordial alignment of density peaks is erased by subsequent non-linear interactions with surrounding matter

Downloaded from https://academic.oup.com/mnras/article-abstract/387/1/128/998214 by University Library user on 19 December 2018

condensations. Voids, however, will be far less affected due their relatively large spatial extent and relatively low density contrast. If anything, their initial alignment will be strengthened by the influence of the large-scale tidal field.

5.2 Void packing

Voids are a unique constituent of the cosmic inventory in that they represent a volume-filling population (Sheth & van de Weygaert 2004). Consequently, the placement of voids in the large-scale matter distribution is a non-trivial issue related to the random object packing problem in mathematics and material's science (see e.g. Conway & Sloane 1998).

We have argued before that an important consequence of the tight packing of voids concerns their shape. As they try to expand outward they will meet up with the surrounding large-scale structures. This involves the surrounding filaments, walls and clusters as well as their neighbouring voids. This strongly restricts their tendency to become more spherical as they expand (Icke 1984; Bertschinger 1985). While the inner cores of voids (van de Weygaert & van Kampen 1993) remain spherical, the surroundings mould them into a generally more flattened configuration. (The shape of regions defined by various level sets in the initial density field is discussed in detail by Shandarin et al. 2006.)

Mathematical studies of the packing problem focus mainly on the packing of equivalent spheres. The more complex problem of ellipsoid packing was recently addressed in a seminal experimental study on the tight packing of (oblately shaped) M&M's (Donev et al. 2004). Not only did they prove that such ellipsoids allow a tighter packing than feasible with purely spherical objects, but also that this goes along with a configuration of strongly aligned ellipsoids (see fig. 1B of Donev et al. 2004).

The situation for the packing of voids is considerably more complex. Cosmic voids have, as we have shown, a considerable diversity in size and shape. Moreover, unlike M&M's, voids are not solid bodies: the void ellipsoids may not be entirely contained within the boundaries of their void patches and as a result may overlap. None the less, we might on purely geometric grounds expect an alignment of a void with its 'natural' neighbours and that, locally, the orientation of voids is strongly constrained by the shape and orientation of its neighbours.

In order to further assess the situation we have analysed four different configurations: a ΛCDM initial Gaussian field, a Poisson field, a regular crystalline configuration and an irregular Voronoi cellular configuration. These reflect one or more aspects of the genuine void distribution (an accompanying publication will provide the details of the study).

In each of these special configurations we see a rapid decline in alignment strength beyond the characteristic void size $R_{\rm v}$, even turning into anticorrelation around $2R_{\rm v}$.

Fig. 3 shows the large-scale correlations for void alignment in the *N*-body model we have studied. We have marked the scales $R_{\rm v}$ and $2R_{\rm v}$ by means of two vertical lines. The fact that in the void sample of this study we find significant alignments beyond $2R_{\rm v}$ is a strong argument for the alignments being due to other factors.

5.3 Large-scale tidal forces

The intricate patterns that constitute the cosmic web are a direct product of the large-scale tidal field (Bond et al. 1996). Voids are an integral part of this pattern and their shape and orientation is expected to react strongly to the surrounding inhomogeneous matter distribution via their tidal influence. The tidal field is a reflection of the underlying inhomogeneous cosmic matter distribution and contains contributions from matter inhomogeneities over a large range of scales.

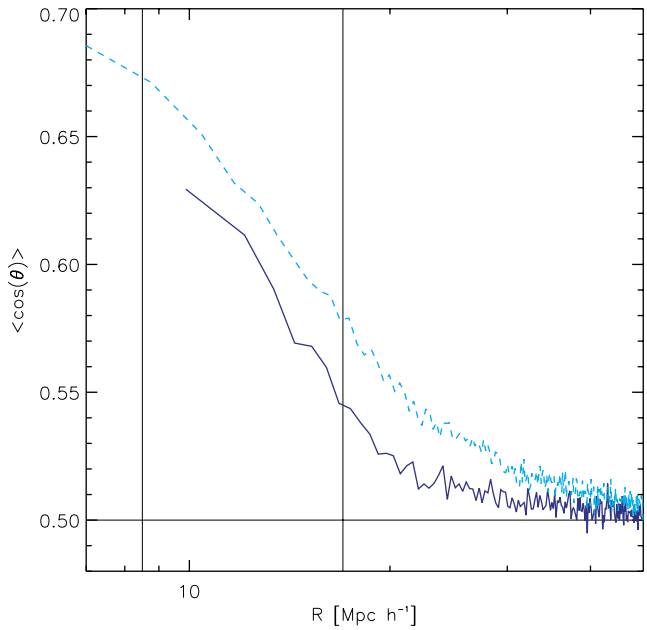

Figure 4. The dotted line shows C_{TS}, the alignment between the compressional direction of the tidal field and the shortest shape axis [cf. equations (4) and (5)]. For comparison, the short axis alignment of Fig. 3 is superimposed.

In a sense, the influence of the tidal field on void orientations is strongly coupled to the initial conditions (see above): already in the initial density field the local shape of a density trough is considerably correlated with the tidal field configurations over a large range of scales.

The key issue is the influence of tidal forces on the evolution of the shape and orientation of voids. This includes the impact on the non-linear development of the void. We are particularly interested in identifying the largest scales over which we can recognize a clear alignment between the tidal field and the orientation of the voids. Their spatial coherence will be crucial for the void–void alignments.

In the next section we will focus on this specific issue.

6 INFLUENCE OF TIDAL FIELD

To test the relationship between the large-scale tidal force field and the void correlations of which they are supposed to be the source we investigate the correlation, at the location of each of the voids, between the tidal tensor $\boldsymbol{T}_{ij}$ and the shape tensor $\boldsymbol{S}_{ij}$.

6.1 Tidal field

We compute the traceless tidal shear components,

$$\boldsymbol{T}_{ij} = \frac{\partial^2\phi}{\partial r_i \partial r_j} - \frac{1}{3}\nabla^2\phi\,\delta_{ij}, \tag{7}$$

for the entire simulation volume. The gravitational potential ϕ, due to the underlying density distribution, is determined from the DTFE density field $\delta(\boldsymbol{r})$ by solving the Poisson equation in Fourier space.

The eigenvalues of the tidal tensor are ordered as $t_1 > t_2 > t_3$, with corresponding unit eigenvectors $\hat{\boldsymbol{e}}_{t_1}$, $\hat{\boldsymbol{e}}_{t_2}$ and $\hat{\boldsymbol{e}}_{t_3}$. We also draw a distinction between the compressional component of the tidal field,

Downloaded from https://academic.oup.com/mnras/article-abstract/387/1/128/998214 by University Library user on 19 December 2018

that part of the tidal field corresponding to the positive eigenvalues of $\boldsymbol{T}_{ij}$, and the dilational component. The compressional component always includes the component $t_1\hat{\boldsymbol{e}}_{t_1}$ while the dilational component always includes $t_3\hat{\boldsymbol{e}}_{t_3}$. Depending on its sign, $t_2\hat{\boldsymbol{e}}_{t_2}$ may contribute to either the compression or to the stretching of the mass element.

6.1.1 Tidal–tidal alignments

In our bid to identify the source of the void–void shape correlations we also need to understand the autocorrelations between the tidal field contributions originating at different scales. To this end we define a *tide–tide* alignment measure $\boldsymbol{A}_{\rm TT}(R_1, R_2)$.

At a location $\boldsymbol{r}$ in the density field we may compare the orientation of the tidal field filtered at two different scales R_1 and R_2, yielding the alignment

$$\Gamma_{\rm TT}(\boldsymbol{r}; R_1, R_2) = \frac{\sum_{i,j} \boldsymbol{T}_{ij}(\boldsymbol{r}; R_1)\, \boldsymbol{T}_{ij}(\boldsymbol{r}; R_2)}{\boldsymbol{T}(\boldsymbol{r}; R_1)\ \boldsymbol{T}(\boldsymbol{r}; R_2)}, \tag{8}$$

where $\boldsymbol{T}\ (\boldsymbol{r}; R_1)$ is the norm of the tidal tensor $\boldsymbol{T}_{ij}(\boldsymbol{r}; R_1)$ filtered on a scale R_1 and $\boldsymbol{T}\ (\boldsymbol{r}; R_2)$ on scale R_2.

The ensemble average of $\Gamma_{\rm TT}(r; R_1, R_2)$ is the tide–tide alignment $\boldsymbol{A}_{\rm TT}(R_1, R_2)$,

$$\boldsymbol{A}_{\rm TT}(R_1, R_2) = \langle\, \Gamma_{\rm TT}(R_1, R_2)\,\rangle. \tag{9}$$

This quantity is computed by taking the average of $\Gamma_{\rm TT}(\boldsymbol{r}; R_1, R_2)$ over a large number of locations $\boldsymbol{r}$. Depending on the average orientations of eigen-axis system the value $A_{\rm TT}(R_1, R_2)$ ranges between $-1 \leqslant A_{\rm TT} \leqslant 1$. Negative values arise when the axis of the largest eigenvalue is aligned with axis of the smallest eigenvalue of the other system. A value of zero would indicate the two samples are uncorrelated.

6.1.2 Void–tidal field alignment: formalism

In order to trace the contributions of the various scales to the void correlations we investigate the alignment between the void shape and the tidal field smoothed over a range of scales R. The smoothing is done in Fourier space using a Gaussian window function $\hat{W}^*(\boldsymbol{k}; R)$:

$$\boldsymbol{T}_{ij}(\boldsymbol{r}; R) = \frac{3}{2}\Omega H^2 \int \frac{{\rm d}\boldsymbol{k}}{(2\pi)^3} \left(\frac{k_i k_j}{k^2} - \frac{1}{3}\delta_{ij} \right) \hat{W}^*(\boldsymbol{k}; R)\, \hat{\delta}(\boldsymbol{k})\, {\rm e}^{-{\rm i}\boldsymbol{k}\cdot\boldsymbol{r}}. \tag{10}$$

Here, $\hat{\delta}(\boldsymbol{k})$ is the Fourier amplitude of the relative density fluctuation field at wavenumber $\boldsymbol{k}$.

We evaluate the alignment $\boldsymbol{A}_{\rm TS}(R_1)$ between the void shape ellipsoid and the local tidal field tensor $\boldsymbol{T}_{ij}(R_1)$, Gaussian filtered on a scale R_1 at the void centres. This is done by evaluating, for every void, the function $\Gamma_{\rm TS}(m, R_1)$ at the void centres:

$$\Gamma_{\rm TS}(m; R_1) = -\frac{\sum_{i,j} \tilde{\boldsymbol{S}}_{m,ij}\, \boldsymbol{T}_{ij}(\boldsymbol{r}_m; R_1)}{\tilde{\boldsymbol{S}}_m\ \boldsymbol{T}(\boldsymbol{r}_m; R_1)}, \tag{11}$$

where $\boldsymbol{T}\ (\boldsymbol{r}_m; R_1)$ is the norm of the tidal tensor $\boldsymbol{T}_{ij}(\boldsymbol{r}_m)$ filtered on a scale R. The void–tidal alignment $\boldsymbol{A}_{\rm TS}(R_1)$ at a scale R_1 is then the ensemble average

$$\boldsymbol{A}_{\rm TS}(R_1) = \langle\, \Gamma_{\rm TS}(R_1)\,\rangle \tag{12}$$

which we determine simply by averaging $\Gamma_{\rm TS}(m, R)$ over the complete sample of voids.

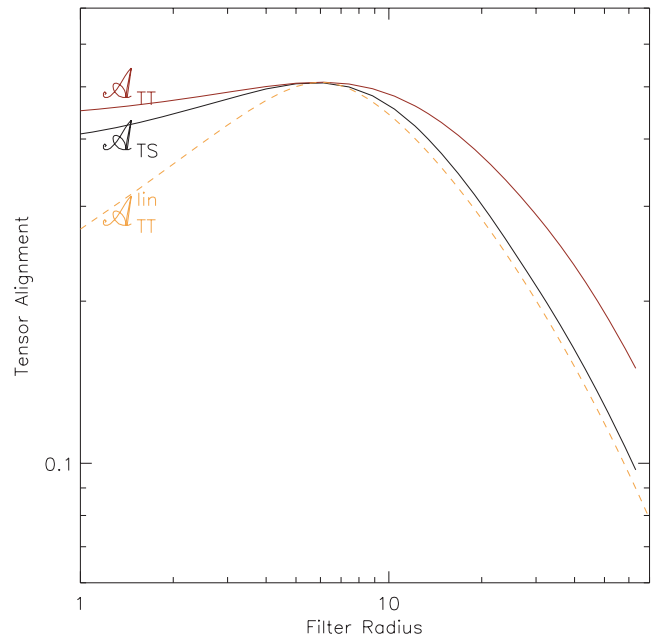

Figure 5. Solid line: the local alignment $\boldsymbol{A}_{\rm TS}(R_1)$ of voids with the tidal field, as a function of the smoothing radius R_1 of the tidal field. Dashed line: alignment $\boldsymbol{A}^{\rm lin}_{\rm TT}\ (R_1, R_2)$ between tidal field on scale $R_2 = 6\,h^{-1}$ Mpc and tidal field on scale R_1 (see text). The relation is based on the prediction for a Gaussian random field with a ΛCDM spectrum. Dot–dashed line: tide–tide alignment $\boldsymbol{A}_{\rm TT}(R_1, R_2)$ measured from the *N*-body simulation described in the text.

6.2 Void–tidal field alignment: results

A visual impression of the strong relation between the void's shape and orientation and the tidal field is presented in the lower right-hand panel of Fig. 1. The tidal field configuration is depicted by means of (red coloured) tidal bars. These bars represent the compressional component of the tidal force field in the slice plane, and have a size proportional to its strength and are directed along the corresponding tidal axis. The bars are superimposed on the pattern of black solid watershed void boundaries, whose orientation is emphasized by means of a bar directed along the projection of their main axis.

The compressional tidal forces tend to be directed perpendicular to the main axis of the void. This is most clearly in regions where the forces are strongest and most coherent. In the vicinity of great clusters the voids point towards these mass concentrations, stretched by the cluster tides. The voids that line up along filamentary structures, marked by coherent tidal forces along their ridge, are mostly oriented along the filament axis and perpendicular to the local tidal compression in these regions. The alignment of small voids along the diagonal running from the upper left to the bottom right is particularly striking.

A direct quantitative impression of the alignment between the void shape and tidal field, may be obtained from Fig. 4. The figure shows $C_{\rm TS}$ (dotted line), the alignment between the compressional direction of the tidal field and the shortest axis alignment (solid line) shows that the tidal field is even stronger aligned. This indicates that the tidal field is instrumental in aligning the voids. To quantify and trace the tidal origin of the alignment we have plotted in Fig. 4 the local shape–tide alignment function $\Gamma_{\rm TS}$ versus the smoothing radius R_1. By smoothing over a scale R_1 we suppress the contribution by mass concentrations and structures with a scale smaller than R_1. Likewise, we have evaluated the tide–tide alignment $\boldsymbol{A}_{\rm TT}(R_1, R_2)$ as

Downloaded from https://academic.oup.com/mnras/article-abstract/387/1/128/998214 by University Library user on 19 December 2018

a function of the same variable filtering scale R_1. The filter scale R_2 (equation 9) is fixed at a value of $R_2 \approx 6\,h^{-1}$ Mpc, slightly smaller than the mean void size. At this scale we expect a strong influence of the local shape on the tidal field, so that this quantity is expected to provide additional information on the dynamical influence of the large-scale tidal field on the dynamics of the void. Note that this implies there to be a slight offset between the actual mean void size, $R_\mathrm{v} \approx 8.5\,h^{-1}$ Mpc, and the peak scale of $\boldsymbol{A}_\mathrm{TS}$. The latter is biased towards the more strongly clustered small voids, whose alignment is often due to one coherent nearby large-scale structure, often a filament or cluster.

The following observations can be made.

(i) The alignment is strong over the whole range of smoothing radii out to $R_1 \approx 20$–$30\,h^{-1}$ Mpc ($\boldsymbol{A}_\mathrm{TS} \approx 0.25$). At $R_1 \approx 25\ h^{-1}$ Mpc the amplitude is still more than half the alignment strength at the peak scale of $R_2 \approx 6\ h^{-1}$ Mpc.

(ii) The alignment peaks at a scale of $R_1 \approx 6\,h^{-1}$ Mpc. This scale is very close to the average void size (see Fig. 2), and also close to the scale of non-linearity. The latter is not a coincidence: the identifiable voids probe the linear–non-linear transition scale.

(iii) There is still a remarkably strong alignment signal at radii larger than $R_1 > 20\,h^{-1}$ Mpc (where $\boldsymbol{A}_\mathrm{TS} \approx 0.3$). It forms a strong argument for the substantial role of the large-scale tidal field in aligning the voids. Local contributions, in particular due to the void's own ellipticity, are only partially responsible for the shape-tidal field alignment: if there were no external large-scale contribution the alignment Γ_TS would have disappeared for smoothing radii R in excess of the average void scale.

We have also analysed higher resolution simulations. The results we found here carry over to the higher resolved simulations. The smaller box of the latter, however, contain fewer voids and there is a smaller range over which the influence of tidal fields can be included. The results do remain significant but are marked by more noise.

6.3 Tidal connections

We have established a strong correlation between void orientation and the large-scale tidal field. We now compare this with the self-alignment of the large-scale tidal field that would be expected on the basis of linear perturbation theory. The dashed curve in Fig. 5 is the linear theory tide–tide alignment $\boldsymbol{A}_\mathrm{TT}^\mathrm{lin}\ (R_1, R_2)$, with $R_1 = 6\,h^{-1}$ Mpc. This function is computed directly from the power spectrum $P(k)$ as

$$A_\mathrm{TT}^\mathrm{lin}(R_1, R_2) = \frac{1}{\sigma_{R_1}\sigma_{R_2}} \int_0^\infty \frac{\mathrm{d}k}{2\pi} k^2 P(k) \hat{W}(k; R_1) W(k; R_2),$$

where $\hat{W}$ is the Fourier transform of the tophat filter. In the equation σ_{R_1} is the root mean square density fluctuation at scale R_1, likewise for σ_{R_2} on scale R_2. On scales greater than the void scale the void–tidal field alignment follows the tidal field alignment. On smaller scales, however, we start to see a marked deviation: the alignments are stronger than expected from the initial linear field. This may be because of non-linear effects on small scales: the tidal field on the smaller scales where the density fluctuations are non-linear is even strong enough to cause the destruction of small voids near the filaments of the cosmic web where there is a strong anisotropic force field (see van de Weygaert, Sheth & Platen 2004).

We also measured the tide–tide alignment $\boldsymbol{A}_\mathrm{TT}(R_1, R_2)$ for the tidal field of our ΛCDM cosmology where any non-linear effects that are present are accounted for. The dot–dashed curve is the result (note that the amplitude has been scaled so that the amplitudes of both $\boldsymbol{A}_\mathrm{TT}$ curves match the peak of the $\boldsymbol{A}_\mathrm{TS}$ curve). The fact that, on small scales, there is clear agreement between the void–tide alignment and the tide–tide alignment underlines the important role of tidal forces throughout the formation history of structures in the cosmic web.

As an incidental remark, the existence of the long range tide–void alignment tells us that the void anisotropy is not a mere artefact of the WVF method chopping spherical voids in two (which would of course lead to non-spherical voids having correlated alignments).

7 CONCLUSION AND DISCUSSION

We have investigated the shapes and alignments of voids found in the large-scale matter distribution of the VLS GIF *N*-body simulation of structure formation in a ΛCDM universe. The void sample has been identified using the WVF technique.

7.1 Overview of results

Although voids tend to be less flattened or elongated than the haloes in the dark matter distribution, they are nevertheless quite non-spherical: they are slightly prolate with axis ratios of the order of $c : b : a \approx 0.5 : 0.7 : 1$. Two important factors contribute to this flattening. Internally, voids tend to become more spherical as they expand (Icke 1984). However, they will never be able to reach perfect sphericity before meeting up with surrounding structures. Furthermore, external tidal forces will contribute substantially to the anisotropic development of the voids. In this study we have established the influence of the tidal fields as being an important agent in the dynamical evolution of voids. Indeed, our study provides strong confirmation that tidal forces dominate the shaping of the Cosmic web, as emphasized long ago by Bond et al. (1996).

We have also investigated the relative orientation of the voids. The orientation of voids appears to be strongly correlated with alignments spanning distances $>30\,h^{-1}$ Mpc. This is true for both the shortest and longest axes of the void shape. This coherence is quite conspicuous in plots of the density distribution. To test for such void alignments in observational data a follow-up study will apply the WVF formalism to galaxy redshift surveys.

We find an intimate link between the cosmic tidal field and the void orientations. Over a range of scales we find a strong alignment of the voids with the tidal field arising from the smoothed density distribution. Given that the alignment correlations remain significant on scales considerably exceeding twice the typical void size, our results show that the long-range external field is responsible for the alignment of the voids. This confirms the view that the large-scale tidal force field is the main agent for the spatial organization of the cosmic web.

7.2 Insights

We have argued that the large-scale tidal field is not only the main agent responsible for the shapes of the voids but also for the resulting alignments of the voids. Locally, the orientation of a void turns out to be strongly aligned with the tidal force field generated by structures on scales up to at least 20–30 h^{-1} Mpc. On scales comparable to the average void size we also found indications of non-linear effects, with the void's orientation reacting to the small-scale non-linear influences.

This conclusion agrees with that of a similar study of halo alignments by Lee et al. (2007). However, the alignment of haloes tends to

Downloaded from https://academic.oup.com/mnras/article-abstract/387/1/128/998214 by University Library user on 19 December 2018

be strongly attenuated by local non-linear effects (e.g. van Haarlem & van de Weygaert 1993; Aragón-Calvo et al. 2007) rendering the final halo alignment signal weaker than that for voids.

One aspect we have not yet addressed in detail is the entanglement of initial conditions and the influence of the tidal field. On large scales, where the density fluctuations are in the linear regime, these are different aspects of the inhomogeneous matter distribution: if one is known the other can be determined. In this respect the indication of non-linear effects in the tidal–void alignment $\boldsymbol{A}_{\rm TS}$ (Fig. 5) at small scales is interesting. They may very well be an expression of the strong influence of coherent overdense filaments and dense compact clusters on the evolution of small voids in the outer regions of large voids.

van de Weygaert et al. (2004) argued that the collapse of small voids, an essential aspect of the hierarchical evolution of voids (Sheth & van de Weygaert 2004), manifests itself in a tidally induced anisotropic contraction of small underdensities at the void boundaries. The dynamics and the fate of these small underdensities are often decisively influenced by external anisotropic forces (van de Weygaert & Babul, unpublished manuscript). While such forces may affect the non-linear evolution of haloes and clusters to a considerable extent (Bond & Myers 1996; Sheth, Mo & Tormen 2001), they do not go as far as deciding their fate.

This work is part of a study of the evolution of voids under the influence of external. A proper framework for following the gradual hierarchical build-up of void regions under the influence of external tidal forces is provided by the void patch description (Bond, Kofman & Pogosyan 1996; Platen, van de Weygaert & Jones, in preparation). To some extent the void patch formalism is a more accurate approximation of reality than for the equivalent peak patch: because of their approximate uniformity void evolution is accurately described by the ellipsoidal model.

A perhaps even more complex issue is that of the identity of the outer regions of voids, the regions where the void merges into the surrounding matter distribution. We have argued that this will play an important role in determining the shape of voids. However, a proper definition of a void boundary does not (yet) exist. Arguably the WVF has proven to represent a major advance along these lines and we should soon be able to be more definite on the issue.

Having established the external influences on a void's evolution, we may try to understand the sensitivity of the void population to the underlying cosmology. This depends to a considerable degree on the differences in scale dependence of the tidal force fields. Lee & Park (2007) did find a considerable influence. This will open the door to the use of voids in determining the global cosmology.

ACKNOWLEDGMENTS

We gratefully acknowledge the use of the Virgo Consortium simulation. We thank Miguel Aragón-Calvo for useful discussions on various technical aspects of this paper and the referee Vincent Desjaques for useful comments.

REFERENCES

Aragón-Calvo M. A., Jones B. J. T., van de Weygaert R., van der Hulst J. M., 2007, ApJ, 655, L5
Bardeen J. M., Bond J. R., Kaiser N., Szalay A. S., 1986, ApJ, 304, 15
Basilakos S., Plionis M., Yepes G., Gottlöber S., Turchaninov V., 2006, MNRAS, 365, 539
Beisbart C., Kersher M., 2000, ApJ, 545, 6
Bertschinger E., 1985, ApJS, 58, 1
Binggeli B., 1982, A&A, 107, 338
Bond J. R., 1987, in Faber S., ed., Nearly Normal Galaxies. Springer-Verlag, New York, p. 388
Bond J. R., Myers S. T., 1996, ApJS, 103, 1
Bond J. R., Kofman L., Pogosyan D., 1996, Nat, 380, 603
Colberg J. M., Sheth R. K., Diaferio A., Gao L., Yoshida N., 2005, MNRAS, 360, 216
Conway A., Sloane I., 1994, Sphere Packings, Lattices and Groups. Wiley, New York
Desjacques V., 2007, preprint (arXiv:0707.4670)
Donev A., Cisse I., Sachs D., Variano E. A., Stillinger F. H., Connelly R., Torquato S., Chaikin P. M., 2004, Sci, 303, 990
Gottlöber S., Łokas E. L., Klypin A., Hoffman Y., 2003, MNRAS, 344, 715
Hahn O., Porciani C., Carollo C. M., Dekel A., 2007, MNRAS, 375, 489
Icke V., 1984, MNRAS, 206, 1
Lee J., Evrard A. E., 2007, ApJ, 657, 30
Lee J., Park D., 2006, ApJ, 652, 1
Lee J., Park D., 2007, preprint (arXiv:0704.0881)
Lee J., Springel V., Pen U.-L., Lemson G., 2007, preprint (arXiv:0709.1106)
Park D., Lee J., 2007a, Phys. Rev. Lett., 98, 1301
Park D., Lee J., 2007b, ApJ, 665, 96
Platen E., van de Weygaert R., Jones B. J. T., 2007, MNRAS, 380, 551
Plionis M., Basilakos S., 2002, MNRAS, 329, L47
Regøs E., Geller M. J., 1991, ApJ, 373, 14
Rhee G., van Haarlem M., Katgert P., 1991, AJ, 103, 6
Romano-Díaz E., van de Weygaert R., 2007, MNRAS, 382, 2
Sahni V., Sathyaprakash B. S., Shandarin S. F., 1994, ApJ, 431, 20
Shandarin S., Feldman H. A., Heitmann K., Habib S., 2006, MNRAS, 376, 1629
Sheth R. K., van de Weygaert R., 2004, MNRAS, 350, 517
Sheth R. K., Mo H. J., Tormen G., 2001, MNRAS, 323, 1
Springel V. et al., 2005, Nat, 435, 629
Stoyan D., Stoyan H., 1994, Fractals, Random Shapes, and Point Fields: Methods of Geometrical Statistics. Wiley, New York
Trujillo I., Carretero C., Patiri S. G., 2006, ApJ, 640, L111
Tully R. B., Shaya E. J., Karachentsev I. D., Courtois H., Kocevski D. D., Rizzi L., Peel A., 2007, preprint (arXiv:0705.4139)
van de Weygaert R., Schaap W. E., 2007, in Martínez V., Saar E., Martínez-González E., Pons-Borderia M., eds, Lectures at Summerschool, Valencia, 2004, Data Analysis in Cosmology. Springer-Verlag, Berlin, p. 129
van de Weygaert R., van Kampen E., 1993, MNRAS, 263, 481
van de Weygaert R., Sheth R., Platen E., 2004, in Diaferio A., ed., IAU Colloq. 195, Outskirts of Galaxy Clusters: Intense Life in the Suburbs. Cambridge Univ. Press, Cambridge, p. 58
van Haarlem M. P., van de Weygaert R., 1993, ApJ, 418, 544

This paper has been typeset from a TEX/LATEX file prepared by the author.

Downloaded from https://academic.oup.com/mnras/article-abstract/387/1/128/998214 by University Library user on 19 December 2018